Numerical simulation of a UV photografting process for hollow-fiber membranes

Tchicaya Goma-Bilongo, Ahmad Akbari, Michaël Clifton, Jean-Christophe Remigy

▶ **To cite this version:**

Tchicaya Goma-Bilongo, Ahmad Akbari, Michaël Clifton, Jean-Christophe Remigy. Numerical simulation of a UV photografting process for hollow-fiber membranes. Journal of Membrane Science, 2006, 2 (1-2), pp.308-317. ⟨10.1016/j.memsci.2005.11.013⟩. ⟨hal-03598007⟩

HAL Id: hal-03598007

https://hal.science/hal-03598007v1

Submitted on 4 Mar 2022

HAL is a multi-disciplinary open access archive for the deposit and dissemination of scientific research documents, whether they are published or not. The documents may come from teaching and research institutions in France or abroad, or from public or private research centers.

L'archive ouverte pluridisciplinaire **HAL**, est destinée au dépôt et à la diffusion de documents scientifiques de niveau recherche, publiés ou non, émanant des établissements d'enseignement et de recherche français ou étrangers, des laboratoires publics ou privés.

HAL Authorization

Numerical simulation of a UV photografting process for hollow-fiber membranes

T. Goma-Bilongo [a], A. Akbari [b], M.J. Clifton [a], J.-C. Remigy [a,*]

[a] *Laboratoire de Génie Chimique (CNRS UMR 5503), Université Paul Sabatier, 31062 Toulouse Cedex 9, France*
[b] *Carpet Department, Faculty of Architecture and Arts, University of Kashan, Kashan, Iran*

Abstract

A numerical model has been developed to represent the process by which hollow-fiber membranes can undergo continuous surface modification by UV photografting. The model takes into account the coupled effects of radiation, mass transfer with polymerization reaction and heat transfer with evaporation. It gives approximately correct values for the mass of polymer grafted, but no attempt is made to relate this quantity with permeability or retention. The behavior of this complex model is used to explain how operating conditions can influence the result of the grafting process.

Keywords: UV photografting; Hollow fiber; Membrane surface modification; Numerical model; Nanofiltration

1. Introduction

Membrane technology is widely used for the production of drinking or process water. This has become an attractive technology in recent years as a possible alternative to conventional treatment processes. It has the advantage of treating natural water with less chemical additives and giving a good-quality product. Hollow-fiber membranes suitable for treatment by ultrafiltration and microfiltration have been available for some time and recent research is oriented towards producing nanofiltration (NF) hollow-fiber membranes.

In this context, a novel route is studied for producing hollow-fiber membranes intended for reducing water hardness: photochemical modification of the outer surface of ultrafiltration (UF) membranes by UV photografting reduces the size of membrane pores and adds electric charges to the surface. UV photografting creates, at the surface of the fiber, a new layer of polymer that is responsible for the new properties of the membrane. This new layer of polymer should be as fine as possible ($\sim$1 μm or even less) in order to obtain good retention of salts and small organic molecules without greatly reducing membrane permeability. This is one of the aspects of the UV photografting process studied in this work.

This technique is easy to implement [1], and also offers the flexibility of producing specifically tailored membranes [2]. UV photografting technology has now been used for producing membranes for different applications, such as the reduction of fouling by natural organic matter during production of potable water [3] and removal of charged organic molecules such as dyes [4].

In the process studied here, the membrane passes through a bath of monomer solution before being irradiated in a UV reactor: this process has the advantage of being a continuous one and it is particularly suited to the treatment of hollow-fiber membranes. Acrylic acid (AA) was selected as the monomer to be grafted because the chemical and physicochemical properties of this monomer are readily available in the literature [5]. The UF membranes used for grafting are made of polysulfone. This material was selected because polysulfone membranes are widely used in industrial applications and present certain advantages such as chemical and physical resistance in use and photosensitivity to UV radiation [6,7]. As the polymer formed, poly(acrylic acid), is highly soluble in water, a cross-linker was included in the monomer solution in order to ensure a correct cohesion of the grafted polymer.

* Corresponding author. Tel.: +33 561557618; fax: +33 561556139.
E-mail address: remigy@chimie.ups-tlse.fr (J.-C. Remigy).

The UV photografting process combines the phenomena of mass transfer, heat transfer and polymerization reaction: we propose in this paper a numerical simulation of this process. This simulation is aimed at providing a better understanding of the coupling between the transfer phenomena (mass and heat transfer) and the polymerization reaction and also represents the influence of the major parameters such as: UV energy dose, monomer concentration and line rate which have recently been studied experimentally [8].

2. Numerical simulation of a UV photografting process

To represent the UV photografting process, the numerical model needs to be able to reproduce the combined effects of the various phenomena. It is a one-dimensional and transitory model. In space, only the radial axis is considered, as the system is regarded as having a symmetry of rotation. The reference axis moves with the fiber: in this way the time co-ordinate also corresponds to a length traversed by the fiber.

The UV photografting process can be divided into three steps (see Fig. 1 and the details of experiments given in Section 3).

2.1. The passage of the fiber through the monomer bath

During this step, the water-saturated fiber, initially free of monomer, comes into contact with a solution of this molecule, at concentration C_b. The only physical phenomenon that takes place in this step is the diffusion of the monomer into the pores of the membrane. We assume that the area porosity of the membrane is equal to its volume porosity and that the tortuosity of the pores is low: the diffusion coefficient then has the same value inside the pores as in the bulk liquid. This assumption means that the diffusion process is independent of the porosity variations within the membrane, which are in any case almost impossible to quantify. The mass transfer by diffusion is described by Fick's second law, with a diffusion coefficient that does not vary with the concentration

$$\frac{\partial C}{\partial t} = D\frac{\partial^2 C}{\partial r^2} \tag{1}$$

The initial conditions ($t=0$) are:

$$r < r_f : \quad C = 0, \qquad r \geq r_f : \quad C = C_b \tag{2}$$

Assuming that the solution outside the pore is continuously renewed, the boundary conditions are ($t>0$):

$$r = 0 : \quad \frac{\partial C}{\partial r} = 0, \qquad r = r_f : \quad C = C_b \tag{3}$$

2.2. The passage of the fiber between the bath and the UV reactor

When the fiber leaves the bath it carries with it a liquid film (of thickness e) on its surface: after a short moment of relaxation, this film moves upwards with the fiber at the same velocity (see Fig. 2). So the liquid is motionless with respect to the axes that move with the fiber. Between the bath and the UV lamps, the monomer continues to diffuse in the pores of the fiber, according to Eq. (1). It should be noted that the liquid film serves as the main source of monomer during the photografting step. Quéré [9] shows that the mode of entrainment of the liquid film can be predicted, depending on the capillary number $Ca = \mu v/\gamma$. This study focuses on only two modes for $Ca < 1$.

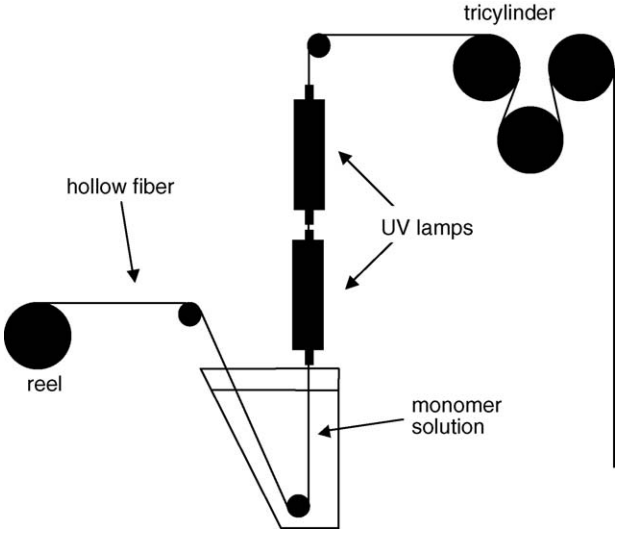

Fig. 1. Continuous photografting set-up used in experiments: schematic diagram.

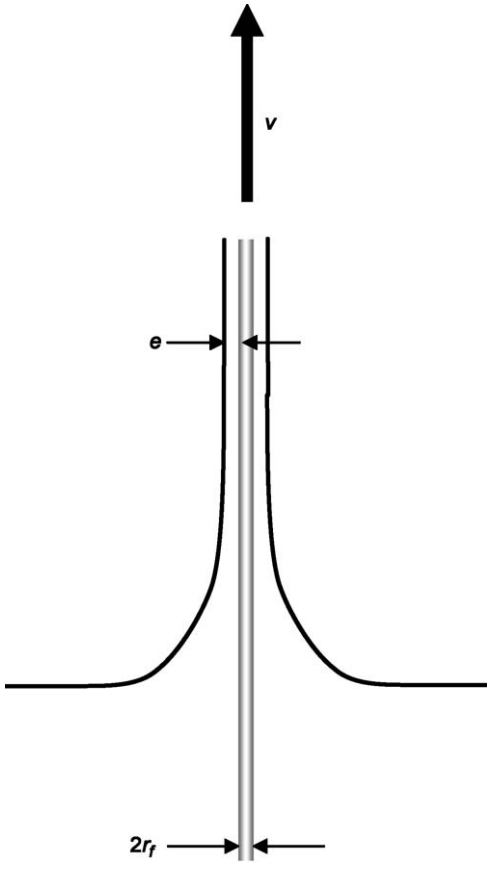

Fig. 2. Entrainment of the liquid film by the hollow fiber.

The first is the visco-inertial mode, which is characterized also by the Weber number $We = \rho v^2 r_f/\gamma$. This mode (for $We < 1$) results from a compromise between viscous forces and the inertia of the liquid. A semi-empirical formula represents the film thickness:

$$e = \frac{r_f Ca^{2/3}}{1 - We} \tag{4}$$

For $We > 1$, only the viscous boundary layer is carried away from the bath by the fiber, particularly at high velocities. The contact time of the fiber in the bath determines the thickness of the film: it increases with the length of the fiber passage in the monomer bath but decreases with velocity. This is the boundary-layer mode, for which the semi-empirical formula for film thickness is as follows:

$$e = \sqrt{\frac{\mu l_b}{\rho v}} \tag{5}$$

When the system is operating under conditions where $We \approx 1$, the value taken for e is the minimum of the values given by these two equations.

Once the fiber leaves the bath, the solution outside the fiber is no longer renewed and there is no mass transfer at the surface of the liquid film: the boundary condition there becomes:

$$r = r_f + e : \quad \frac{\partial C}{\partial r} = 0 \tag{6}$$

2.3. The passage of the fiber through the UV reactor

In this last step, the monomer continues to diffuse inside the membrane pores. In addition, the radiation from the UV lamps creates radicals on the surface of the polymer and thus starts a radical polymerization reaction. Finally, the infra-red part (IR) of the radiation heats the fiber and causes a progressive evaporation of the liquid film (see Fig. 3). So there is now coupling between mass transfer, heat transfer and the polymerization reaction

$$\frac{\partial C}{\partial t} = D\frac{\partial^2 C}{\partial r^2} - R_A \tag{7}$$

where R_A is a source term representing the rate of the radical polymerization reaction:

$$R_A = k_p C\sqrt{\frac{\phi I_a}{k_t}} \tag{8}$$

The quantum yield ϕ for this reaction is taken as 0.5. The rate constants k_p and k_t and their variation with temperature have been previously published [5]. So far in this work, we have neglected the effects of homopolymerization and the UV degradation of the polysulfone membrane.

Inside the membrane, the UV radiation, of intensity q_{uv}, is propagated in the negative r direction and is absorbed by the polysulfone according to a law of the Beer-Lambert type:

$$\frac{dq_{uv}}{dr} \propto q_{uv} \tag{9}$$

If we define a penetration depth l_{UV} as the distance at which 99% of the radiation has been absorbed, then we obtain the following variation of light intensity in the radial direction:

$$\frac{q_{uv}}{q_{UV}} = \exp\left[-\frac{\alpha(r_f - r)}{l_{UV}}\right] \tag{10}$$

where $\alpha = -\ln(0.01) \approx 4.605$.

Here q_{UV} is the intensity arriving at the fiber surface. The penetration depth was determined by measuring the UV intensity transmitted (UVB and UVC) by polysulfone membranes of increasing thickness: it was found that for a thickness of 10 μm the radiation transmitted was barely measurable using a radiometer from Hönle UV France, Lyon, France. So the penetration depth has been taken equal to 10 μm.

The rate of absorption of the radiation $|dq_{uv}/dr|$ is related to the molar source of photons I_a taking part in the photochemical reaction:

$$I_a = \frac{1}{h\nu N_A}\left|\frac{dq_{uv}}{dr}\right| \tag{11}$$

By combining Eqs. (10) and (11), we obtain the expression:

$$I_a = q_{UV}\frac{\lambda}{hcN_A}\frac{\alpha}{x_{UV}}\exp\left[-\frac{\alpha(r_f - r)}{l_{UV}}\right] \tag{12}$$

Our measurements showed that most of the UV radiation is absorbed by polysulfone at wavelengths around 300 nm: this is the wavelength used in our calculations [8].

The fiber is of small diameter and filled with an aqueous medium that is a quite good conductor of heat: so its thermal inertia is low. This means that the temperature of the fiber can be taken as uniform in the radial direction, so that there is always an equilibrium between the heat arriving by IR radiation from the lamps and the heat taken up by evaporation. The temperature of evaporation is fixed in such a way that the saturating vapor pressure is sufficient to evacuate by diffusion a vapor flux capable of cooling the fiber via the latent heat of evaporation. It is

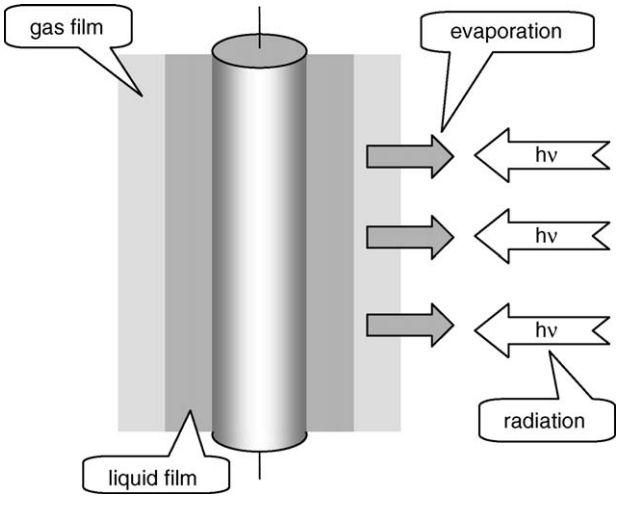

Fig. 3. Coupling of the mass transfer, heat transfer and radiation phenomena around the fiber.

worth noting that the temperature of evaporation has an influence on polymerization kinetics and on certain physical properties of the monomer solution (viscosity, surface tension).

The evaporation flux is controlled by the thickness δ of the mass-transfer layer surrounding the fiber. This quantity is extremely difficult to estimate. The mass transfer of the vapor near the fiber depends on the gas flow in that zone and this in turn is made up of a number of contributions: the laminar flow induced by the linear movement of the fiber, the injection effect created by the flow of the vapor itself, natural convection of both thermal and solutal origin and finally the vibration of the fiber. It seems likely that the latter effect dominates. As calculation from the fundamental phenomena seems impossible, the only way of estimating this parameter was from its effect in the model: too high a value means slow evaporation and unrealistically high fiber temperatures, while too low a value means that the evaporation is so fast that the fiber surface dries up. The fiber temperature near the outlet of the reactor was observed in an approximate way using an IR camera and found to lie in the range 30–40 °C, only varying slightly with line rate. Also the fiber was always seen to leave the reactor with a moist surface. We have assumed a fixed value of 665 μm as best suiting these different observations.

At the liquid/vapor interface an equilibrium is established. The mole fraction of monomer in the liquid at the interface is given by:

$$x_{aa} = \frac{C^e}{C^e + (\rho - C^e M_{aa})/M_w} \tag{13}$$

The corresponding vapor mole fraction y_{aa} can be calculated from an empirical formula based on published data [10]. The molar concentration of monomer in the vapor phase is then calculated assuming an ideal-gas behavior for the monomer vapor:

$$\tilde{C}_{aa} = \frac{y_{aa} p^0_{aa}}{RT} \tag{14}$$

For the water vapor, the molar concentration is calculated from the virial equation:

$$\tilde{C}_w = \frac{p_w/RT}{\frac{1}{2} + \sqrt{\frac{1}{4} + \beta p_w/RT}} \tag{15}$$

The molar flux for each vapor component i through the mass-transfer layer is determined by its molar vapor concentration at the vapor/liquid interface and in the environment (the operation room):

$$J_i = \frac{D_i(\tilde{C}^e_i - \tilde{C}^{env}_i)}{\delta} \tag{16}$$

For the monomer, the environmental concentration $\tilde{C}^{env}_{aa}$ is 0, while the water vapor concentration is fixed by the relative humidity: $p^{env}_w = Up^0_w$.

There is continuity of these fluxes at the interface and the monomer flux represents the limiting condition for Eq. (7) at the interface, at $r = r_f + e$:

$$J_{aa} = -D \left.\frac{\partial C}{\partial r}\right|_{r=r_f+e} \tag{17}$$

The values of the interface fluxes make it possible to obtain expressions for the interface velocity (due to evaporation):

$$-\frac{de}{dt} = J_{aa} V_{aa} + J_w V_w \tag{18}$$

and for the heat flux absorbed by evaporation:

$$q_{vap} = \Delta H^{vap}_w J_w + \Delta H^{vap}_{aa} J_{aa} \tag{19}$$

The radiation energy flux emitted by the lamps was measured (using the radiometer previously mentioned) as a function of the electrical power P, in the range $3300\ W < P < 5500\ W$: it was found to fit the following empirical formula:

$$q = 974P - 2026 \tag{20}$$

The energy flux is distributed among various zones of the spectrum. The two zones of interest here are the infra-red and the ultra-violet, for which the manufacturer of the lamps indicates the following ratios: $q_{IR} = 0.4q$ and $q_{UV} = 0.3q$. For the infra-red ratio, our experimental observations on drying of the fiber indicate that the effective ratio is approximately $q_{IR} = 0.03q$. Whereas the manufacturer's figure is related to the radiation emitted by the lamp, the actual heating of the fiber can be lower because of a low absorbancy of the fiber and because the UV reactor is equipped with cold-mirror reflectors which minimize reflection of IR radiation.

Equilibrium between the IR radiation energy and the heat consumed by evaporation is expressed as:

$$q_{IR} - q_{vap} = 0 \tag{21}$$

The temperature of the fiber is fixed so that this equilibrium is always respected.

Eq. (7) is discretized using the finite-volume method [11] with cylindrical control volumes to give a completely implicit linear system for the discrete values of monomer concentration.

At each time step it is assumed that part or whole of the outermost volume element is removed from the liquid film by evaporation. If the rate of evaporation is high, the outermost volume element is entirely removed and the time step Δt is fixed in the following way:

$$\Delta t = -\frac{\Delta e}{J_{aa} V_{aa} + J_w V_w} \tag{22}$$

where Δe is the thickness of the outermost volume element.

For lower evaporation rates the time step is chosen so as to maintain numerical errors within tolerable limits:

$$\frac{D\Delta t}{[\min(\Delta r)]^2} \leq 5 \tag{23}$$

This model particularly allows calculation of the evolution of the monomer concentration profile, as well as the quantity of monomer grafted. The latter quantity is an integral of the quantity of polymer formed at each point inside the fiber. We also

calculated the fraction of monomer consumed by the polymerization reaction (reaction yield) and by evaporation.

3. Experiment

The membranes to be modified were supplied by Polymem S.A. (Toulouse, France). They were ultrafiltration hollow fibers (HF) in polysulfone, 720 μm in diameter, and were characterized by an initial hydraulic permeability of 46 L h^{-1} m^{-2} bar^{-1} and a MWCO of around 20 kDa according to the manufacturer.

AA and the cross-linker *N*,*N*′-methylene bis acrylamide are used as received from Aldrich. AA concentration is given in mass percent, whereas cross-linker concentration is given in mole percent with respect to the molar concentration of AA.

The experimental method was as follows: the hollow fiber was washed with reverse-osmosis (RO) treated water. Then it was installed in the UV photografting pilot, where it passed at a given line rate through a monomer bath having a suitable concentration before being irradiated by two polychromatic UV lamps (FOZFR 250) in a UV reactor with elliptical mirrors (UVAPRINT LE). Both lamps and reactor were purchased from Hönle UV France, Lyon, France. The modified membrane was then washed with RO treated water.

The quantity of monomer grafted can be determined from the ion-exchange capacity, as each molecule of monomer grafted adds one ion-exchange site. The protocol was as follows. An approximately 1 m length of fiber was cut and soaked for 24 h in a 2 M hydrochloric solution in order to convert all the cation-exchange sites into H^+ form. After rinsing in RO treated water for 24 h, the fiber was soaked in 0.1 M NaCl whose pH was adjusted to a value of 2, i.e. well below the pK_a of the acrylic acid. The cation-exchange sites are titrated by a 0.1 M NaOH solution. In such a titration, the ion exchanger remains insoluble, but comes to equilibrium with the solution to which the titrant is added. The neutralization of the fiber can be observed by recording the pH of the supernatant solution while the titration is in progress [12]. The mass of polymer grafted was determined from the following expression:

$$m_p = (V_1 - V_2)\frac{CM_{aa}}{l_f}$$

where l_f is the length of the fiber, C the molar concentration of NaOH solution, and V_2 is the volume of NaOH solution necessary to neutralize the acid in the initial NaCl solution, while V_1 is the volume necessary to neutralize both the fiber and the initial acid.

4. Results and discussion

This section presents various calculated results that can improve the understanding of the UV photografting process. Firstly operating parameters that have an impact on the grafting are identified and the grafting zone is situated. In a second part, we present the tendencies for the pilot used and propose some perspectives for future work.

Several authors [13,14] claim that the UV photografting process is determined only by the UV energy dose and the monomer concentration in the reaction zone. In the present work, the numerical model is used to decide whether this observation is still true for continuous grafting on hollow-fiber membranes.

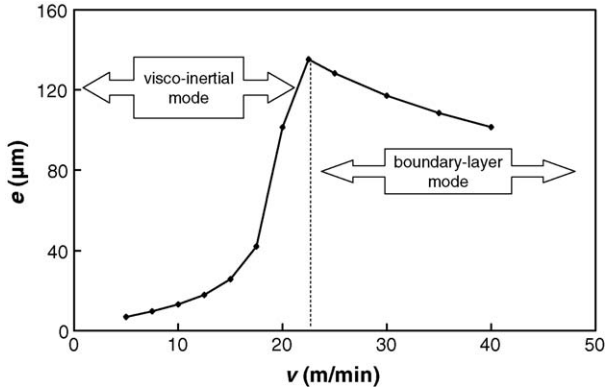

Fig. 4. Thickness of the liquid film as a function of line rate for $C_b = 10$ wt.%.

4.1. Thickness of liquid film

As mentioned in Section 2, the liquid film acts as a reserve of monomer in the photografting step, so the variation of film thickness with line rate is an important element in the process. Fig. 4 shows the thickness of liquid film as a function of the line rate. For line rates below 20 m/min the Weber number is less than 1, so the thickness of the liquid film increases strongly with line rate: this is characteristic of the visco-inertial mode of entrainment. But for line rates above 20 m/min ($We > 1$), the thickness of liquid film decreases, as the film is entrained in the boundary-layer mode.

4.2. Profile of monomer concentration

Fig. 5 shows the monomer concentration profile at different times during the three steps of the UV photografting process. On leaving the monomer bath (a), the fiber carries a liquid film on its surface: the monomer concentration is constant in the liquid film

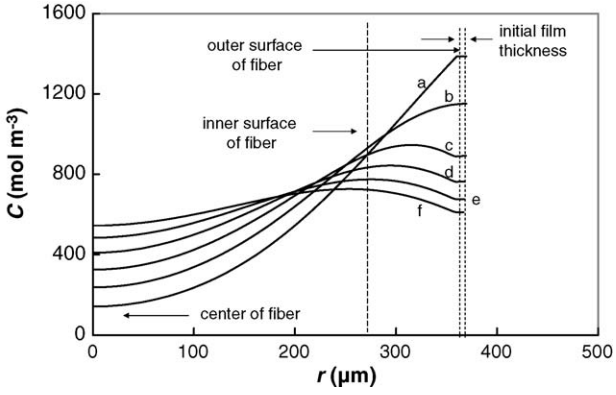

Fig. 5. Profile of monomer concentration at different times during the passage of the fiber through the pilot plant: $C_b = 10$ wt.%; $v = 7.5$ m/min; $L = 0.5$ m. (a) Exit of the monomer bath; (b) entrance of the UV reactor; (c) first quarter of UV reactor; (d) second quarter of UV reactor; (e) third quarter of UV reactor; (f) exit of UV reactor.

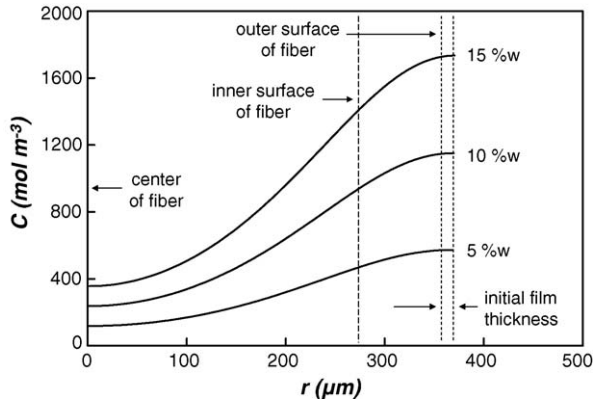

Fig. 6. Profile of monomer concentration at the entrance of the UV reactor for different values of C_b the initial monomer concentration: $v = 7.5$ m/min.

but decreases progressively towards the center of the fiber as the monomer diffuses into the pores. Between the moment when the fiber leaves the monomer bath and its entry into the UV reactor (b), the monomer concentration decreases at the surface of the fiber as the monomer continues to diffuse into the pores. When the fiber is irradiated in the UV reactor, part of the liquid film is evaporated and part of the remaining monomer is consumed by the polymerization reaction, whose kinetics varies with the temperature of vaporization of the monomer solution. Four curves (c–f) show the evolution of the monomer concentration profile during the passage through the reactor. The consumption of the monomer is visible here as a progressive erosion of the concentration profile near the surface: in this case, there is a beginning of monomer deficiency in the grafting zone.

In Figs. 6–8, we will focus on the monomer concentration profile at the entrance to the UV reactor: this profile has a great impact on the polymerization reaction (in particular in situating the grafting zone) as well as on the evaporation of the liquid film. The aim here is to identify the different parameters that influence this profile.

4.2.1. *Effect of the monomer concentration*

Fig. 6 shows that the thickness of liquid film does not vary much with the monomer concentration in spite of the effect of

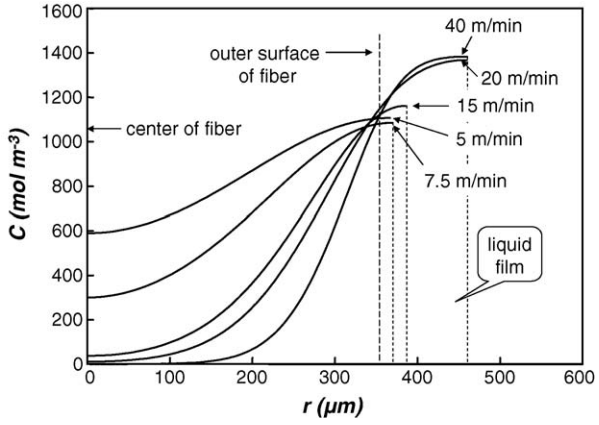

Fig. 7. Profile of monomer concentration at the entrance of the UV reactor for different values of the line rate: $C_b = 10$ wt.%.

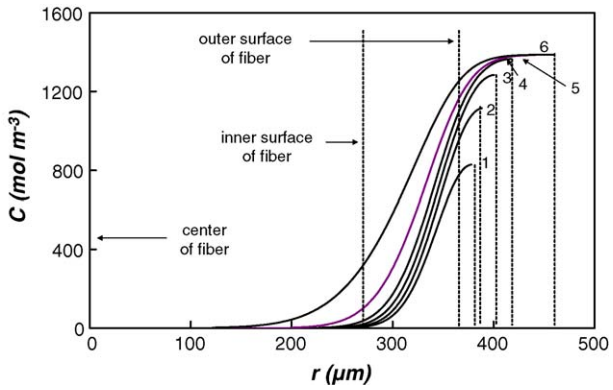

Fig. 8. Profile of monomer concentration at the entrance of the UV reactor for different heights of the monomer bath: $C_b = 10$ wt.%; $v = 40$ m/min. (1) $h_b = 0.02$ m; (2) $h_b = 0.05$ m; (3) $h_b = 0.1$ m; (4) $h_b = 0.2$ m; (5) $h_b = 0.4$ m; (6) $h_b = 0.6$ m.

the monomer concentration on solution properties (viscosity and surface tension). But the increase in monomer concentration at the surface of fiber increases the monomer concentration in the reaction zone.

4.2.2. *Effect of line rate*

Fig. 7 also shows the monomer concentration profile at the reactor entrance: it can be seen how strongly the thickness of the liquid film varies with the line rate. For line rates between 5 and 7.5 m/min, the monomer concentration up to a depth of 10 μm inside the fiber (the radiation zone) is approximately equal to that of the liquid film on the fiber surface. The flat profile of monomer concentration is explained by strong monomer diffusion into the fiber. This is related to the residence time of the fiber in the monomer bath. For line rates above 20 m/min, it is observed that the monomer does not penetrate into the center of the fiber because the residence time in the monomer bath is short.

4.2.3. *Effect of the height of the monomer bath*

In Fig. 8, it can be seen how the thickness of liquid film varies with the height of the monomer bath for $v = 40$ m/min. This is characteristic of the boundary-layer mode. It should be recalled that in the visco-inertial mode, the thickness of the liquid film does not vary with the height of the bath as it is a function of the capillary and Weber numbers only. It can also be seen that there is a height of the bath beyond which the monomer concentration profile at the entrance of the reactor varies only slightly.

4.3. *Concentration profile of grafted polymer*

Now that the various parameters capable of modifying the concentration profile at the inlet of the reactor have been identified, this section will be devoted to locating the zones where grafting occurs so as to define the best conditions for grafting.

4.3.1. *Effect of the monomer concentration*

The concentration profile of polymer formed inside the fiber as a function of the radial co-ordinate, is shown in Fig. 9 for different values of the initial monomer concentration. This should

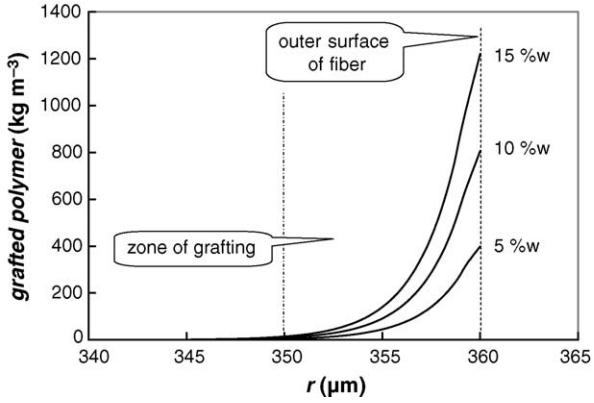

Fig. 9. Concentration profile of the grafted polymer for different values of the initial monomer concentration: $v = 7.5$ m/min; $L = 0.5$ m.

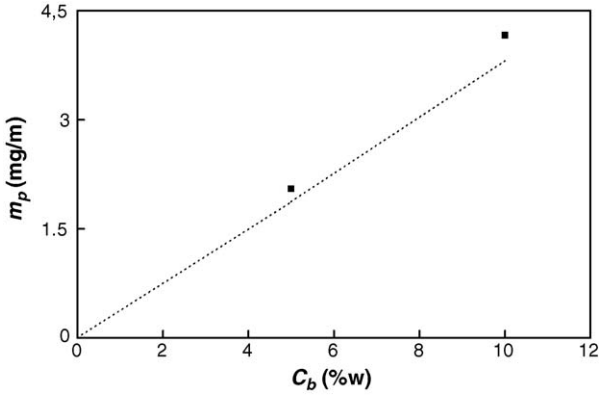

Fig. 11. Mass of grafted polymer as a function of the initial monomer concentration: comparison of simulated values (given by the curve) and experimental values (shown as points): $v = 7.5$ m/min; $L = 0.5$ m.

be compared with Fig. 6 which shows that the monomer concentration profile in the grafting zone is relatively flat at the inlet to the reactor. However in Fig. 9 the concentration of polymer grafted decreases roughly exponentially: this shows that it is essentially proportional to the quantity of UV radiation absorbed by the fiber. Monomer is heavily consumed at the surface and within a depth of 5 μm into the fiber for each monomer concentration. Beyond 5 μm, as the light intensity is much lower, much less polymer is formed. But for a high monomer concentration ($C_b = 15$ wt.%), the value of the concentration of grafted polymer approaches the density of pure poly acrylic acid (1200–1500 kg m^{-3}) [5]. This excessively high value probably corresponds to a case where, in the experimental situation, a layer of poly(acrylic acid) is formed at the fiber surface. A layer on this sort was detected in recent observations by X-ray micro-tomography. This thick surface grafting is similar in mechanism to homopolymerization and so is not provided for in the present model. To take account of this phenomenon would require the introduction of extra adjustable parameters.

Fig. 10 shows that the quantity of monomer grafted increases almost linearly with the initial monomer concentration. This is due to the reaction rate of photo-polymerization Eq. (8), which is proportional to the monomer concentration for a given amount UV energy absorbed and due to the fairly small variations in monomer concentration in the grafting zone where the monomer is present in excess.

For a given velocity, so for a given dose of UV energy, Fig. 11 shows the quantity of monomer grafted as a function of the initial monomer concentration: the results of the numerical model are compared with experimentally measured values. It can be seen that, at least under these conditions, the prediction of the model is approximately correct.

4.3.2. *Effect of line rate*

Fig. 12 shows how the profile of polymer grafted varies with line rate; it should be compared with Fig. 7 which shows that the line rate has little effect on the monomer concentration in the reaction zone. This result suggests that the amount of UV energy absorbed is the essential parameter here in the photografting process as it is strongly dependent on the residence time in the reactor. However Fig. 13 allows this reasoning to be qualified: it shows the quantity of monomer grafted as a function of the line rate. The effect of the film thickness (Fig. 4) is visible in the quantity of monomer grafted. For line rates between 5 and 15 m/min, the quantity of monomer grafted decreases with increasing line rate. This is because the increase in line rate reduces the residence time in the UV reactor, thus reducing the quantity of UV energy absorbed and so the quantity of monomer

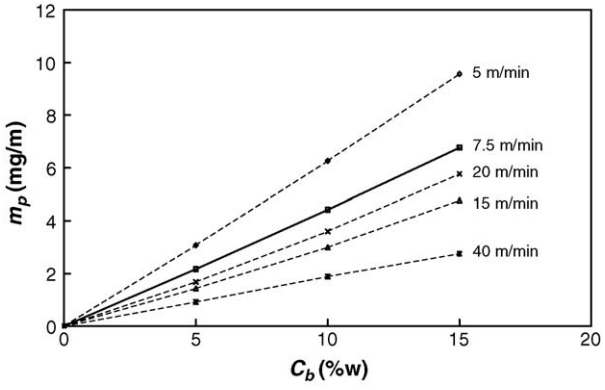

Fig. 10. Mass of grafted polymer as a function of the initial monomer concentration for different values of the line rate: $L = 0.5$ m.

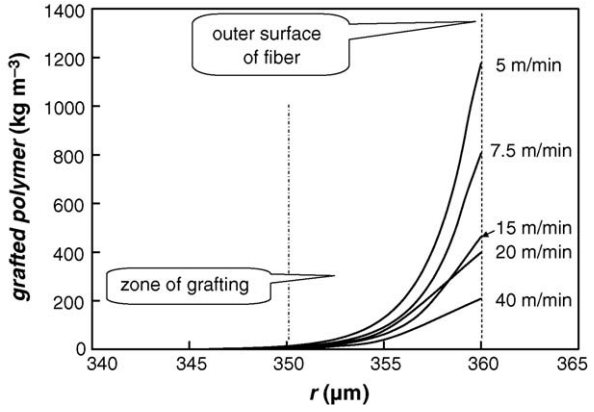

Fig. 12. Concentration profile of the grafted polymer for different values of the line rate: $C_b = 10$ wt.%; $L = 0.5$ m.

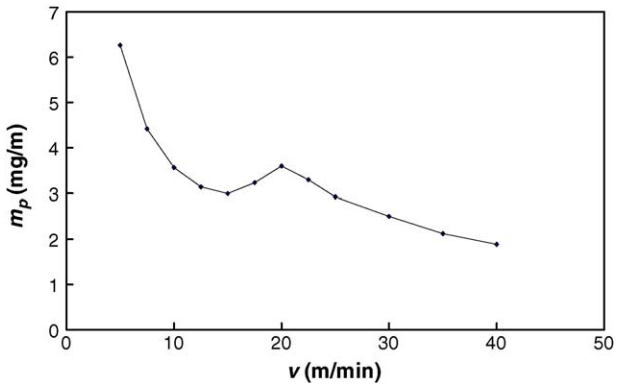

Fig. 13. Mass of grafted polymer as a function of the line rate: $C_b = 10$ wt.%; $L = 0.5$ m.

grafted. So in this range it is UV energy absorbed that controls the degree of grafting. In a second zone (15–40 m/min), the quantity of monomer grafted first rises then falls with increasing line rate. The initial rise is explained by the rapid increase in thickness of the liquid film in the upper part of visco-inertial mode (see Figs. 4 and 7): it is capable of compensating for the decrease in the UV energy received by the fiber because the thicker film acts as a reserve of monomer that replenishes the reaction zone as monomer is consumed. So the thickness of liquid film controls the grafting in this zone. Beyond the maximum, the decrease in the quantity grafted reflects both the decrease in film thickness (because of the transition to the boundary-layer mode of entrainment) and the shorter residence time.

4.3.3. Effect of the height of the monomer bath

In Fig. 14, the concentration profile of grafted polymer is shown for different heights of the monomer bath in the boundary-layer entrainment regime ($v = 40$ m/min): the grafting on the fiber surface increases because both the thickness of the liquid film and the residence time in the monomer bath increase.

Fig. 15 also shows that the quantity of monomer grafted increases with the height of the monomer bath. For line rates below 20 m/min, this increase is simply due to increasing residence time in the monomer bath, which in its turn modifies the monomer concentration profile at the entrance of the UV reactor. On the other hand for line rates above 20 m/min, the thickness of liquid film varies with the height of the monomer bath, as shown in Fig. 8. The quantity of monomer grafted at $v = 20$ m/min, varies only slightly especially for small heights of the monomer bath: this is certainly due to the presence of a thick liquid film on the fiber surface.

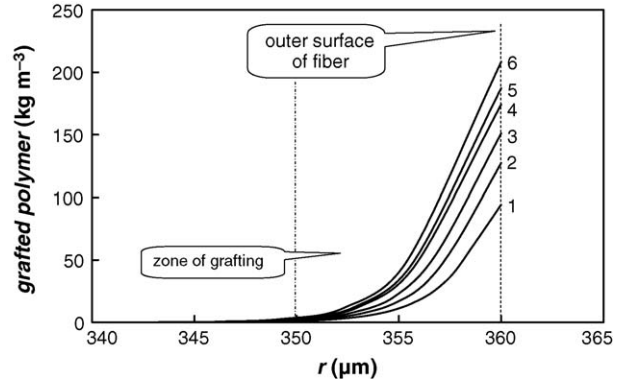

Fig. 14. Concentration profile of the grafted polymer for different values of the height of the monomer bath: $C_b = 10$ wt.%; $v = 40$ m/min; $L = 0.5$ m. (1) $h_b = 0.02$ m; (2) $h_b = 0.05$ m; (3) $h_b = 0.1$ m; (4) $h_b = 0.2$ m; (5) $h_b = 0.4$ m; (6) $h_b = 0.6$ m.

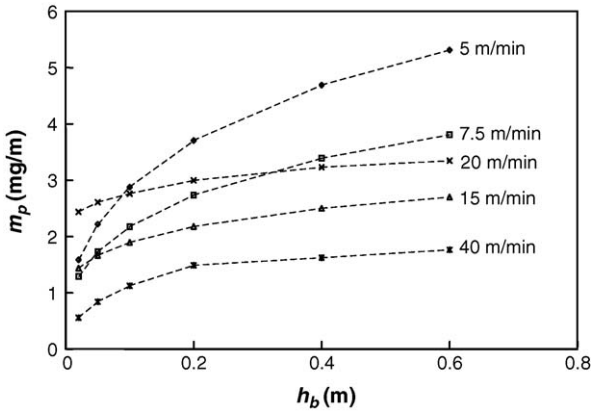

Fig. 15. Mass of grafted polymer as a function of the height of the monomer bath for different values of the line rate: $C_b = 10$ wt.%; $L = 0.5$ m.

4.3.4. Effect of the reactor length

The concentration profile of polymer formed is shown in Fig. 16 for different reactor lengths. The amount of grafting on the fiber increases with the residence time of the fiber in the reactor, as is shown also in Fig. 17. Increasing the length of the reactor means increasing the UV energy absorbed by the fiber. It is likely that for much longer residence times, the variation could become non-linear, when the monomer in the film starts to be used up. The continuous, almost linear, increase given here by the simulation can be explained by the presence of an excess of monomer both inside the fiber and in the liquid film; the monomer remains in excess in spite of the increase in length of the UV reactor. In Fig. 17, the effect of film thickness is also visible, via the effect of the line rate.

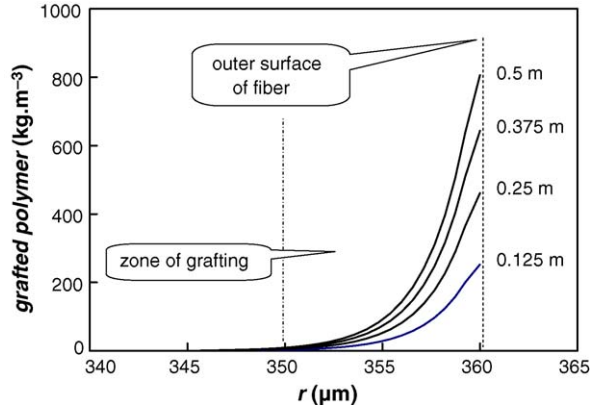

Fig. 16. Concentration profile of the grafted polymer for different values of the length of UV reactor: $C_b = 10$ wt.%; $v = 7.5$ m/min.

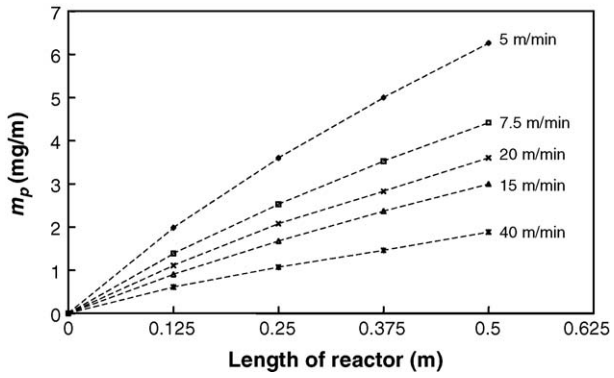

Fig. 17. Mass of grafted polymer as a function of the length of UV reactor for different values of the line rate: $C_b = 10$ wt.%; $L = 0.5$ m.

4.4. Tendencies for engineering the process

The results presented make it possible to predict the tendencies for the pilot used. The reaction yield is very low (5–22%) for all grafting conditions tested here: none of the observed tendencies would allow a significant improvement of this result. This suggests that a production plant similar to the present pilot might require a system allowing the monomer to be recovered and recycled. The only alternative that can be imagined would be to use a different system that could apply the monomer solution to the fiber surface in a very thin film. However there are also some advantages in having the monomer present in large excess.

The numerical model shows that the thickness of the polymer layer formed is about 5 μm whereas nanofiltration hollow fibers should have a fine selective layer (about 1 μm or less). In the present calculations the thickness is essentially determined by the penetration depth of the UV radiation. To obtain a thinner grafting zone, it may be desirable to use less intense radiation over a longer residence time.

Otherwise within the possibilities of the present pilot, the dense polymer grafting necessary to produce nanofiltration membranes is produced by a high monomer concentration in the reaction zone and a strong dose of UV energy. This can be achieved either by working at a low line rate (long residence times in the bath and in the reactor) or by increasing the length of the reactor. The advantage of working at low line rates is to create a thin liquid film and enhance diffusion of the monomer into the fiber. This could be a good choice for producing affinity membranes, which require in-depth grafting. On the other hand, operation at higher line rates is limited in the present pilot by the maximum length of the reactor which is 0.5 m. However the only advantage of working at high line rates, is that the monomer does not penetrate into the center of fiber (as shown in Fig. 7): our calculations show that this does little to increase the reaction yield. These conditions could be suitable for manufacturing membranes of the low-fouling type and ultrafiltration membranes (UF) modified which do not require dense grafting.

5. Conclusion

The numerical simulation presented here has allowed a better understanding of the photografting process and made it possible to identify the key parameters involved in it. It has also indicated the existence of optimum operating conditions for obtaining dense grafting. It should be remembered that it is in any case difficult to establish a link between the quantity of monomer grafted and the performance of the modified fiber in terms of permeability and solute retention. The simulation shows that it is desirable to work at a low line rate for which it is the residence time in the reactor that controls the grafting. This model also allows the zone of grafting to be situated inside the fiber. It would be interesting to compare these results with experimental observations where the zone of grafting is revealed by filtering a suspension of colloidal gold prior to detection by scanning electron microscopy.

The present model has numerous deficiencies and in future developments the homopolymerization reaction, in particular, will have to be included in it. But it already gives approximately correct amounts of grafted polymer for a series of monomer concentrations: this suggests that the model as it now stands is not too far from reality. Other future work will compare experimental and predicted values of the quantity of monomer grafted while varying other parameters, particularly the UV energy dose. This will eventually lead to a numerical model capable of optimizing the conditions for modifying hollow fibers by UV photografting.

Acknowledgements

This study was financially supported by European community and a doctoral grant from the government of Congo-Brazzaville. The authors thank Philippe Aptel for helpful discussions.

Nomenclature

c	speed of light ($m\,s^{-1}$)
C	concentration of acrylic acid in solution ($mol\,m^{-3}$)
Ca	capillary number
$\tilde{C}_i$	concentration of i in vapor phase ($mol\,m^{-3}$)
D	diffusion coefficient of acrylic acid in solution ($m^2\,s^{-1}$)
D_{aa}	diffusion coefficient of acrylic acid in air ($m^2\,s^{-1}$)
D_w	diffusion coefficient of water in air ($m^2\,s^{-1}$)
e	thickness of liquid film (m)
E_{UV}	UV energy ($J\,cm^{-2}$)
h	Planck's constant (J s)
h_b	height of monomer bath (m)
ΔH_i^{vap}	molar enthalpy of vaporization of i ($J\,mol^{-1}$)
I_a	photon source ($mol\,m^{-3}\,s^{-1}$)
J_i	molar flux of i ($mol\,m^{-2}\,s^{-1}$)
k_p	propagation coefficient ($m^3\,mol^{-1}\,s^{-1}$)
k_t	termination coefficient ($m^3\,mol^{-1}\,s^{-1}$)
l_b	length of fiber passage in the monomer bath (m)
l_{UV}	penetration depth (m)

L	length of the UV reactor (m)
m_{p}	mass of grafted polymer ($\mathrm{kg\,m^{-1}}$)
M_i	molar mass of i ($\mathrm{kg\,mol^{-1}}$)
N_A	Avogadro constant ($\mathrm{mol^{-1}}$)
p_i	partial pressure of i in vapor phase (Pa)
p_i^0	saturated vapor pressure of i (Pa)
P	electrical power (W)
q	radiation intensity ($\mathrm{W\,m^{-2}}$)
q_{vap}	thermal power consumed by evaporation ($\mathrm{W\,m^{-2}}$)
r	radial co-ordinate (m)
r_{f}	radius of the fiber (m)
R	perfect gas constant ($\mathrm{J\,K^{-1}\,mol^{-1}}$)
R_{A}	rate of the radical polymerization reaction ($\mathrm{mol\,m^{-3}\,s^{-1}}$)
t	time (s)
T	temperature (°K)
U	relative humidity
v	line rate ($\mathrm{m\,min^{-1}}$)
V_i	partial molar volume of i ($\mathrm{m^3\,mol^{-1}}$)
We	Weber number
x_i	mole fraction of i in the liquid phase
y_i	mole fraction of i in the vapor phase

Greek letters

β	second virial coefficient ($\mathrm{m^3\,mol^{-1}}$)
γ	surface tension of monomer solution ($\mathrm{N\,m^{-1}}$)
δ	thickness of gas film (m)
λ	wavelength of radiation (m)
μ	dynamic viscosity of monomer solution (Pa s)
ν	frequency of radiation ($\mathrm{s^{-1}}$)
ρ	density of the monomer solution ($\mathrm{kg\,m^{-3}}$)
ρ_{w}	water density ($\mathrm{kg\,m^{-3}}$)
ϕ	quantum yield

Subscripts

aa	acrylic acid (monomer)
b	monomer bath (initial concentration)
f	fiber
IR	infra-red
UV	ultra-violet
w	water

Superscripts

e	value at vapor/liquid interface
env	value in surrounding environment

References

[1] M. Taniguchi, J.M. Kilduff, G. Belfort, Low fouling synthetic membranes by UV-assisted graft polymerisation: monomer selection to mitigate fouling by natural organic matter, J. Membr. Sci. 222 (2003) 59–70.

[2] J. Pieracci, J.V. Crivello, G. Belfort, Photochemical modification of 10 kDa polyethersulfone ultrafiltration membranes for reduction of biofouling, J. Membr. Sci. 156 (1999) 223–240.

[3] J.E. Kilduff, S. Mattaraj, J.P. Pieracci, G. Belfort, Photochemical modification of poly(ether sulfone) and sulfonated poly(sulfone) nanofiltration membranes for control of fouling by natural organic matter, Desalination 132 (2000) 133–142.

[4] A. Akbari, S. Desclaux, J.-C. Remigy, P. Aptel, Treatment of textile dye effluent using a new photografted nanofiltration membrane, Desalination 149 (2002) 101–107.

[5] J. Braudrup, E.H. Immergent, E.A. Grulke, Polymer Handbook, 4th ed., Wiley–Interscience, New York, 1998.

[6] H. Yamagishi, J.V. Crivello, G. Belfort, Development of a novel photochemical technique for modifying poly(arylsulfone) ultrafiltration membranes, J. Membr. Sci. 105 (1995) 237–247.

[7] G.J. Summers, M.P. Ndawuni, C.A. Summers, Dipyridyl functionalized polysulfones for membrane production, J. Membr. Sci. 226 (2003) 21–33.

[8] S. Béquet, Procédé de photogreffage en continu de membranes fibres creuses, Ph.D. Dissertation, Université Paul Sabatier, Toulouse, France, 2003.

[9] D. Quéré, Fluid coating a fiber, Annu. Rev. Fluid (1999) 347–384.

[10] J. Gmehling, U. Onken, Vapor–Liquid Equilibrium Data Collection: Aqueous-Organic System, Chemistry Data Series, vol. I, part 1, Dechema, Frankfurt, 1977.

[11] S.V. Patankar, Numerical Heat Transfer and Fluid Flow, Hemisphere, New York, 1980.

[12] F. Helfferich, Ion Exchange, McGraw-Hill, New York, 1962.

[13] B. Kaeselev, J. Pieracci, G. Belfort, Photoinduced grafting of ultrafiltration membranes: comparison of poly(ether sulfone) and poly(sulfone), J. Membr. Sci. 194 (2001) 245–261.

[14] C. Qui, F. Xu, Q.T. Nguyen, Z. Ping, Nanofiltration membrane prepared from cardo polyetherketone ultrafiltration membrane by UV-induced grafting method, J. Membr. Sci. 255 (2005) 107–115.